NPL
National Physical Laboratory

NPL REPORT IR 63

CALCULATING ELECTRON PERTURBATION FACTORS FOR ROOS AND NACP-02 IONISATION CHAMBERS

MIRIAM BARRY, DAVID SHIPLEY AND GRAHAM BASS

JULY 2023

Calculating electron perturbation factors for Roos and NACP-02 ionisation chambers

Miriam Barry, David Shipley and Graham Bass
Medical, Marine and Nuclear Department

ABSTRACT

Recent changes recommended in the ICRU Report 90 document (updated from ICRU Report 37) were implemented into the measurement services provided by NPL. With respect to the therapy-level electron calibration service, perturbation factors (to account for the cavity and chamber wall material) needed to be updated. New stopping power ratios were also calculated. This report outlines the relevant Monte Carlo simulations carried out for this purpose.

ISSN 1754-2952

DOI: https://doi.org/10.47120/npl.npl.IR63

National Physical Laboratory
Hampton Road, Teddington, Middlesex, TW11 0LW

This work was funded by the UK Government's Department for Science, Innovation & Technology through the UK's National Measurement System programmes.

Approved on behalf of NPLML by
Russell A S Thomas, Science Area Leader.

CONTENTS

1 INTRODUCTION

This document describes work carried out in support of the calibration service provided by NPL (in its capacity as a Primary Standards Laboratory) for the absorbed dose to water for therapy level electrons. The focus of this report is on the revision of the various factors (perturbation and stopping power ratio) and also the incorporation/inclusion of parameters published in ICRU Report 90 (1) that have been updated from the older version of the document, ICRU Report 37 (2).

The calibration service is described by McEwen *et al.*(1998) (3) but will be described briefly here. The report only mentions the use of an NACP-02 chamber as at the time of writing; although the Roos looked to be a promising option, there was insufficient historical data to support its use. Enough time has elapsed and data has been collected and now the Roos (alongside the NACP-02) has been designated for use in the IPEM code of practice (2003) (4). This was after collection of data and evaluation of perturbation factors, ion recombination and polarity corrections, where these chambers performed the best. In the first instance dose is measured using calorimetry and compared (via substitution) against several reference chambers at the calibration reference depth, z_{ref}. The calibration reference depth is calculated as per the electron code of practice (4), where $R_{50,D}$ is the depth at which dose drops to 50%, see Equation 1.

$$z_{ref} = 0.6 \cdot R_{50,D} - 0.1\ cm$$

Equation 1

Measurements are performed in graphite and a calibration factor ($N_{\text{ref},g}$) for each NPL reference chamber is calculated from Equation 2, where D_g is the absorbed dose to graphite as measured by the graphite calorimeter and $M_{\text{ref,g}}$ is the NPL reference chamber reading.

$$N_{\text{ref},g} = \frac{D_g}{M_{\text{ref},g}}$$

Equation 2

The user chamber calibration factor for calculating dose to water can then be determined through an intercomparison (in water) with the NPL reference chambers. The factor is calculated using Equation 3, where $M_{\text{ref},w}$ is a reference chamber reading in water, $M_{\text{user},w}$ is the user chamber reading in water, $p_{\text{ref},w}$ and $p_{\text{ref},g}$ are the perturbation factors of the reference chamber in water and graphite respectively and $s_{w/\text{air}}$ and $s_{g/\text{air}}$ are the stopping power ratios between water and air and graphite and air respectively.

$$N_{\text{user},w} = N_{\text{ref},g} \frac{M_{\text{ref},w}}{M_{\text{user},w}} \frac{p_{\text{ref},w}}{p_{\text{ref},g}} \frac{s_{w/\text{air}}}{s_{g/\text{air}}}$$

Equation 3

The reference chamber perturbation factors are in fact a combination of contributing factors, namely the cavity perturbation and the chamber wall perturbation. The cavity perturbation is due to the presence of the air cavity within the chamber and the wall perturbation results from the non-water or non-graphite material in the walls of the chamber (depending on whether the measurement is carried out in water or graphite respectively). Previously it was thought that the chamber perturbation in graphite and in water were almost identical and therefore the ratio of the two was assumed to be unity. However with recent advances in Monte Carlo codes, calculation of these factors is possible and as such work was carried out at NPL by Bailey *et al.* in 2015 (5) to investigate this. Bailey *et al.* used Monte Carlo simulations of both dose and stopping power ratio which were then compared to depth ionisation curves measured at NPL using the clinical linac. Cavity perturbation factors (p_{cav}) and wall perturbation factors (p_{wall}) were simulated separately at different depths between $0.1\times R_{50,D}$ and $1.1\times R_{50,D}$. Bailey's paper highlighted the depth dependence of perturbation correction factors and therefore the importance of correcting depths for the materials in the front face of the chambers used. This was taken into consideration in the extension to Bailey's work that is described in this report.

This work was a continuation of the previous work (5) and EGSnrc input files from Bailey were used with only minor adjustments made to the input files for the user code DOSRZnrc where necessary. The linac source models used were identical. In this later study only the overall conversion factor from absorbed dose to graphite to absorbed dose to water, $p_{Q,}$ was calculated (Equation 6), calculated from the ratio of the individual perturbation factors in water and graphite (Equation 4 and Equation 5 respectively), not the separate factors, p_{wall} and p_{cav}. $D_{chamber,w}$ and $D_{chamber,g}$ is the dose to the measurement volume of the fully modelled chamber located at the reference depths in water and graphite respectively, and D_w and D_g is the dose to water and graphite respectively at the reference depths in the absence of the chamber. Also, only the reference depth, z_{ref} (as calculated by Burns' formula, (1)) was investigated. In addition, the new recommended parameters published in ICRU Report 90 were available and were implemented in the simulations. This is described in the NPL Report IR 55 (Bass *et al.*, 2019, (7)) which covers all calibration services provided by the Medical Physics groups at NPL. Given the need to update the service due to the implementation of the recommended ICRU Report 90 parameters, other factors unrelated to ICRU Report 90 were also reviewed.

$$p_{Q,w} = \frac{D_w}{D_{\text{chamber,w}} \cdot s_{w/\text{air}}} \qquad \text{(water)}$$

Equation 4

$$p_{Q,g} = \frac{D_g}{D_{\text{chamber,g}} \cdot s_{g/\text{air}}} \qquad \text{(graphite)}$$

Equation 5

$$p_Q = \frac{p_{Q,w}}{p_{Q,g}} \cdot s_{w/g} \equiv \frac{D_w}{D_{\text{chamber},w}} \cdot \frac{D_{\text{chamber},g}}{D_g}$$

Equation 6

2 METHOD

Monte Carlo simulations were performed using the user codes BEAMnrc, DOSRZnrc and SPRRZnrc that form part of the EGSnrc code system (8). A model of the clinical Elekta Synergy linac in current use at NPL (and used for the electron calibration service) had been previously developed and verified, (5) and was used for this study.

2.1 MATERIALS DATASET

Initially the materials dataset (PEGS4) used previously in Bailey's study (5) were updated to incorporate the new recommended parameters published in ICRU Report 90. The main differences between ICRU Report 37 and ICRU Report 90 (relating to the electron perturbation factors) were the mean excitation energies of both water (I_w) and graphite (I_g). For I_g, the recommended value increased from 78 eV ± 4 eV in ICRU Report 37 to 81 eV ± 1.8 eV in ICRU Report 90. For I_w, the value increased from 75 eV ± 2 eV in ICRU Report 37 to 78 eV ± 2 eV in ICRU Report 90. In addition to the updated mean excitation energies, the material properties were also updated. ICRU Report 90 recommends using the crystalline density of graphite which is 2.265 g·cm^{-3} when evaluating the density effect and using 0.9982 g·cm^{-3} for the density of liquid water. Therefore, in order to implement these recommendations, the material datasets were updated incorporating this new information.

2.2 DEPTH DOSE CALCULATION IN WATER/GRAPHITE

The depth dose curves for electron energies 4, 6, 10, 12, 15 and 20 MeV were calculated using DOSRZnrc in a water and graphite phantom using the materials data set outlined in 2.1. Simulations were carried out using the existing BEAMnrc source models with a 14 cm × 14 cm applicator for the graphite depth dose curves and 20 cm × 20 cm applicator for the water depth dose curves. Source to Surface Distance (SSD) were at 100 cm for both water and graphite simulations. The outer radius of both phantoms was 8 cm the inner scoring region diameter was 0.5 cm with the minor exception that for energies of 15 MeV and above, a slightly larger phantom radius of 15cm was used for the water simulations. The phantom radius of 8cm was used for both the graphite and water simulations at lower energies as it has been shown that percentage depth dose is not impacted by field size. Therefore, percentage depth dose data collected in the inner scoring region will not be affected by the phantom radius if sufficient scatter conditions exist in the adjacent region. The phantom comprised of 200 slabs with thicknesses of either 0.03 cm or 0.06 cm with an overall thickness of 9 cm for the graphite phantom and slab thicknesses of either 0.05 cm and 0.1 cm with an overall thickness of 15 cm for the water phantom. The thinner slabs were positioned so that they were in the region of the depth dose curve slope to enable the intercept and gradient of the linear portion of the slope to be calculated which in turn allowed $R_{50,D}$ (depth at which dose drops to 50%) and z_{ref} to be calculated as per the electron code of practice (4), see Equation 1. z_{ref} values were calculated for both graphite and water for all electron energies and compared to the original z_{ref} values obtained previously based on ICRU Report 37 data.

2.3 STOPPING POWER RATIO CALCULATIONS

Stopping power ratios (SPR) were required for the calculation of the $p_{Q,w}$ and $p_{Q,g}$ values, see Equation 4 and Equation 5. Using the z_{ref} values determined, simulations were performed using SPRRZnrc for Roos and NACP-02 chambers in both graphite or water to determine the stopping power ratio in the region of the measuring volume for each chamber. The restricted Spencer-Attix SPR is calculated between the material assigned and air for the spectrum of particles in the sensitive volume. The chamber in phantom geometry was used (with minor adjustment of the scoring slab thickness: 0.0355 cm and 0.02 cm for water and graphite respectively) but with all materials set to either graphite or water of equivalent thickness, see Figures 1(b). and 2(b). Additionally, for both 15 MeV and 20 MeV water simulations, the phantom radius was increased to 15 cm, see Appendix A. As in the perturbation factor calculations (see Section 2.4), the difference between the water- or graphite-equivalent thicknesses and the physical thickness preceding the chamber volume were determined and these values were used to adjust the SSD of the set up to ensure that source to chamber distance were the same between the different measurement conditions for a particular chamber/energy combination. The source to chamber distance used was 100 cm + z_{ref} (in terms of water/graphite equivalent). An applicator field size of 20 × 20 cm was used for the water simulations and 14 × 14 cm field size used for the graphite simulations. The SPR was scored in the slab corresponding to the chamber measuring volume with the radius of the defined geometry equal to that of the sensitive volume, i.e. 0.5 cm and 0.78 cm for the NACP-02 and Roos chambers respectively. z_{ref} was positioned such that it was at the centre of the scoring slab. The number of SPRRZnrc simulation events used in each calculation were approximately 1e9.

2.4 PERTURBATION FACTOR CALCULATIONS

Using the z_{ref} values determined, simulations were performed using DOSRZnrc for Roos and NACP-02 chambers in either graphite or water to determine the dose deposited in the measuring volume within the chamber, $D_{\text{chamber,g}}$ and $D_{\text{chamber},w}$ respectively. Chamber geometry and materials used in the simulations for the two chambers are represented in Figures 1(b) and 2(b). In the first instance, all materials preceding the air gap were converted to water equivalent or graphite equivalent thicknesses (depending on the measurement conditions) and a suitable amount of build-up added to ensure that the

chamber reference plane was located at depth z_{ref} in terms of equivalent thickness (in either graphite or water). These conditions are referred to as the *full chamber* conditions in either water or graphite. An SSD of 100 cm was used for all full chamber simulations. An applicator field size of 20 × 20 cm was used for the water simulations and 14 × 14 cm field size used for the graphite simulations. The dose was scored in the slab corresponding to the sensitive air volume of the chamber geometry, i.e. within a radius of 0.5 cm and 0.78 cm for the NACP-02 and Roos chambers respectively.

Simulations were also performed using the same chamber geometries outlined above but with all materials replaced with either graphite or water referred to as *graphite-only* or *water-only* conditions respectively. The water only conditions are shown for both Roos and NACP in Figure 1(a) and Figure 2(a) respectively. Scoring of the doses to graphite, D_g, and water, D_w, was carried out in a thin scoring slab of the same radius as the sensitive air volume of the different chambers. However to compensate for the different materials used, i.e. either water or graphite in place of air, the thickness of the scoring slab was adjusted. For the calculations in water the slab thickness was adjusted to 0.0355 cm and for graphite, to 0.02 cm. In the full chamber simulations, the physical thickness preceding the air gap is different to the water/graphite equivalent thickness. Therefore in the water- or graphite-only simulations, to account for these discrepancies, the SSD was adjusted to maintain the same source to chamber reference plane distance. This was achieved by modifying the BEAMnrc input files and either increasing or decreasing the final air gap that is positioned after the gantry head. In the graphite- or water-only simulations, z_{ref} was positioned such that it was at the centre of the scoring slab, not at the boundary closest to the surface as per the full chamber simulations. The number of DOSRZnrc simulation events used in each calculation were approximately 1e9. The full beam source option was used in DOSRZnrc to run the BEAMnrc simulations with the global transport parameters for electrons AE and ECUT set to 0.521 MeV and global parameters for photons AP and PCUT set to 0.01 MeV.

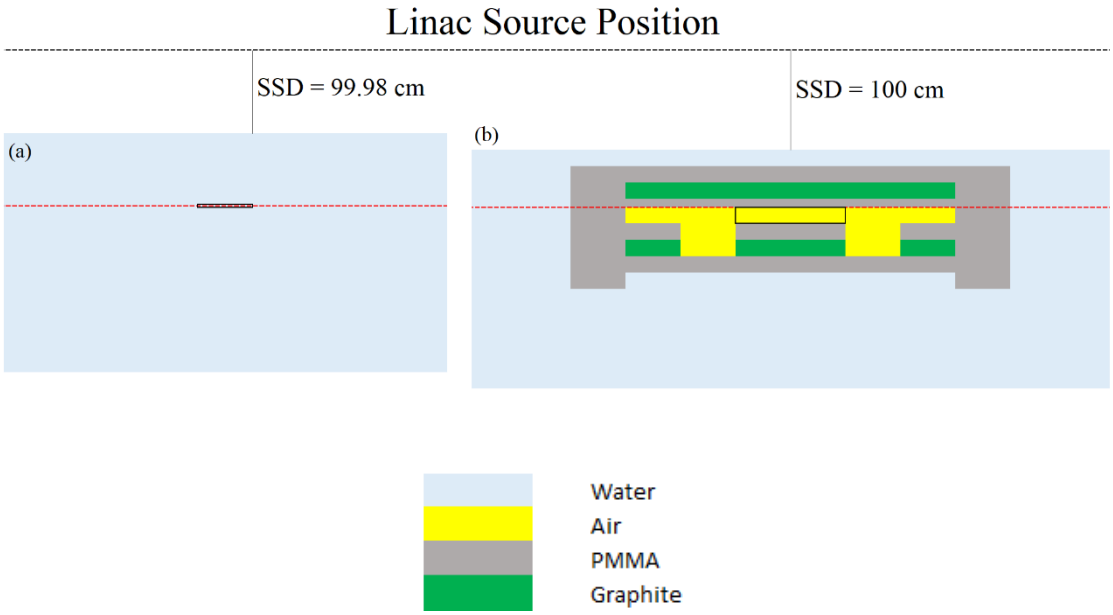

Figure 1. Diagram showing the Roos simulation geometry for (b) the full geometry in water condition and (a) the water-only condition where all regions have been set to water. The red dashed line represents the position of the z_{ref} chamber reference plane which is set just before the measuring air volume in (b) and at the mid-point of scoring slab for the all-water condition (a). The scoring region is represented by the bold outline for both conditions. Diagrams are not to scale.

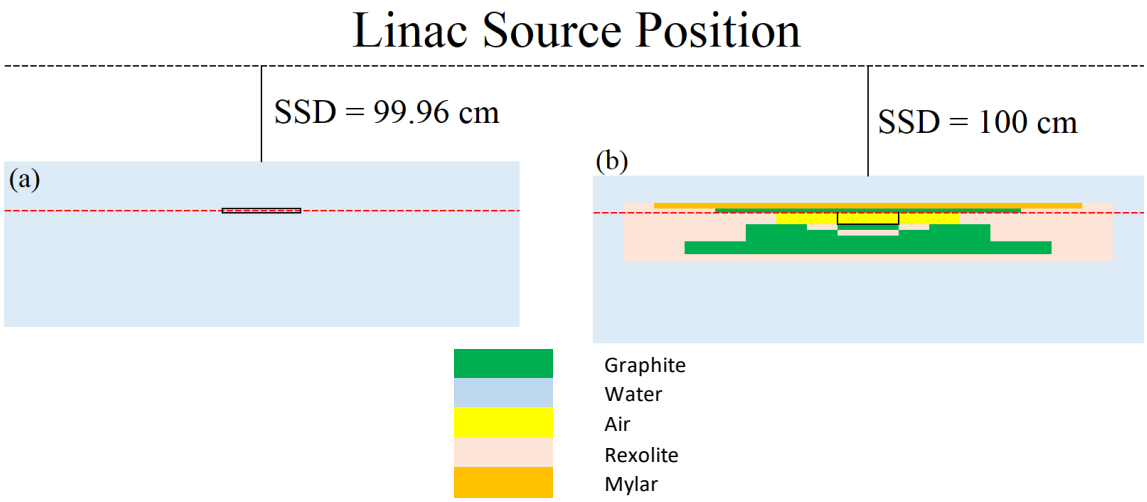

Figure 2. Diagram showing the NACP-02 simulation geometry for (b) the full geometry in water condition and (a) the water-only condition where all regions have been set to water. The red dashed line represents the position of the z_{ref} plane which is set just before the measuring air volume in (b) and at the mid-point of scoring slab for the all-water condition (a). The scoring region is represented by the bold outline for both conditions. Diagrams are not to scale.

3 RESULTS

3.1 DEPTH DOSE CALCULATIONS IN GRAPHITE/WATER

z_{ref} data were collected for the simulated depth dose curves in both water and graphite and were found to be comparable to the data previously collected related to ICRU Report 37 parameters, see Table 1. As the differences were so small it was decided to use the original z_{ref} values to allow minimal changes to be made to the input files used. It was later observed however, that the differences between the ICRU Report 37 and ICRU Report 90 water simulations were mostly as a result of the change in density of water, from 1 g·cm^{-3} to 0.9982 g·cm^{-3}, this difference is displayed in the ICRU Report 37 (corrected) column of Table 1. In hindsight it would have been more appropriate to adjust the z_{ref} for the water simulations. This oversight was investigated to ensure that the impact of the slight discrepancy in z_{ref} (maximum observed was 0.17mm) was not significant in the overall perturbation factor calculated. This is discussed in Section 3.3.

3.2 STOPPING POWER RATIO CALCULATIONS

Stopping power ratio simulation data were collected for each chamber and measurement condition combination. The results are displayed in Figure 3 and Tables 2 to 5 in terms of SPR between the material being assessed and air. Uncertainties displayed are as reported on the SPRRZnrc output file. For cases where multiple simulations were carried out the combined error was calculated in quadrature. Errors displayed are Type A and quote the standard uncertainty expressed as a percentage of the mean (k=1).

Table 1. Summary of z_{ref} values calculated in graphite and water using both ICRU Report 37 and ICRU Report 90 data.

Graphite				
	z_{ref} (cm)		Difference	
E (MeV)	ICRU37	ICRU90	cm	%
4	0.589	0.591	0.002	0.33%
6	0.864	0.864	0.001	0.10%
10	1.542	1.545	0.002	0.15%
12	1.814	1.816	0.002	0.09%
15	2.291	2.292	0.001	0.03%
20	3.115	3.118	0.003	0.09%

Water					
	z_{ref} (cm)			Difference ICRU37 *v.* ICRU90	
E (MeV)	ICRU37	ICRU37 (corrected)	ICRU90	cm	%
4	0.891	0.892	0.893	0.003	0.29%
6	1.315	1.318	1.318	0.002	0.17%
10	2.365	2.369	2.371	0.006	0.24%
12	2.784	2.789	2.786	0.002	0.07%
15	3.438	3.444	3.445	0.008	0.22%
20	4.783	4.792	4.800	0.017	0.35%

3.3 PERTURBATION FACTOR CALCULATIONS

Perturbation factors in water ($p_{Q,w}$) and in graphite ($p_{Q,g}$) were calculated for Roos and NACP-02 chambers and results are displayed in Tables 2 to 5 and Figures 4 and 5. The final factors for use in converting from dose to graphite to dose to water, p_Q are displayed in Figures 6 and 7 and in Tables 6 and 7. The error over all the simulations was calculated in quadrature. All errors displayed are Type A and quote the standard uncertainty expressed as a percentage of the mean (k=1). For the majority of the Roos calculations the statistical uncertainty in the calculation was sufficiently low such that only a single simulation was required for each energy and set of conditions. However, for the NACP-02 chamber, the uncertainties were generally larger and therefore additional simulations were performed to increase the number of events and therefore bring down the uncertainty in the calculated factor. To reduce the uncertainties to a similar size as observed in the Roos data, four additional simulations using the full chamber geometry and one additional simulation in the all graphite set up were carried out. However, with respect to the Roos factors calculated in graphite, there were some anomalies in the trend (some points did not follow a smooth curve and discontinuities were observed) and therefore additional simulations were performed for this set up but only at specified energies where this occurred, these being 4, 6 and 20 MeV. This was to reduce the statistical uncertainty and to further clarify the data trend. For all additional simulations performed, different random number seeds were used for both BEAMnrc and DOSRZnrc to ensure all simulations were independent.

The impact of the small discrepancies in z_{ref} discussed in Section 3.1 were investigated by carrying out additional simulations at the correct z_{ref} for 15 MeV for both the NACP-02 and Roos chambers in water. Within the uncertainty of the simulation and calculation, the differences observed were negligible.

Table 2. Summary of results for Roos chamber simulations in water. All errors displayed are Type A and quote the standard uncertainty expressed as a percentage of the mean (k=1).

Energy (MeV)	Dose [Gy/source particle] full geometry ($D_{chamber}$)	Error	Dose [Gy/source particle] to water (D_w)	Error	$s_{w/air}$	Error	$D_w/D_{chamber}$	$p_{Q,w}$	$p_{Q,w}$ error
4	5.449E-14	0.09%	6.025E-14	0.06%	1.086	0.002%	1.106	1.018	0.11%
6	6.506E-14	0.10%	7.083E-14	0.07%	1.073	0.002%	1.089	1.014	0.12%
10	1.258E-13	0.10%	1.332E-13	0.07%	1.050	0.003%	1.059	1.009	0.12%
12	1.277E-13	0.10%	1.343E-13	0.07%	1.044	0.004%	1.051	1.007	0.12%
15	1.175E-13	0.08%	1.226E-13	0.08%	1.036	0.007%	1.043	1.007	0.11%
20	2.091E-13	0.08%	2.153E-13	0.08%	1.021	0.005%	1.030	1.009	0.11%

Table 3. Summary of results for Roos chamber simulations in graphite. All errors displayed are Type A and quote the standard uncertainty expressed as a percentage of the mean (k=1).

Energy (MeV)	Dose [Gy/source particle] full geometry ($D_{chamber}$)	Error	Dose [Gy/source particle] to graphite (D_g)	Error	$s_{g/air}$	Error	$D_g/D_{chamber}$	$p_{Q,g}$	$p_{Q,g}$ error
4	5.445E-14	0.09%	5.213E-14	0.06%	0.946	0.002%	0.957	1.013	0.11%
6	6.447E-14	0.09%	6.097E-14	0.07%	0.935	0.002%	0.946	1.011	0.11%
10	1.266E-13	0.10%	1.171E-13	0.07%	0.916	0.003%	0.925	1.009	0.12%
12	1.279E-13	0.10%	1.176E-13	0.07%	0.911	0.003%	0.920	1.009	0.12%
15	1.690E-13	0.10%	1.540E-13	0.07%	0.903	0.004%	0.911	1.009	0.12%
20	2.138E-13	0.11%	1.929E-13	0.08%	0.893	0.006%	0.902	1.010	0.14%

Table 4. Summary of results for NACP-02 chamber simulations in water. All errors displayed are Type A and quote the standard uncertainty expressed as a percentage of the mean (k=1).

Energy (MeV)	Dose [Gy/source particle] full geometry ($D_{chamber}$)	Error	Dose [Gy/source particle] to water (D_w)	Error	$s_{w/air}$	Error	$D_w/D_{chamber}$	$p_{Q,w}$	$p_{Q,w}$ error
4	5.475E-14	0.05%	6.033E-14	0.07%	1.086	0.002%	1.102	1.015	0.08%
6	6.528E-14	0.07%	7.087E-14	0.07%	1.073	0.002%	1.086	1.012	0.10%
10	1.261E-13	0.06%	1.333E-13	0.07%	1.050	0.003%	1.057	1.007	0.09%
12	1.279E-13	0.07%	1.342E-13	0.07%	1.044	0.003%	1.050	1.006	0.10%
15	1.175E-13	0.11%	1.226E-13	0.12%	1.036	0.007%	1.044	1.008	0.16%
20	2.095E-13	0.09%	2.156E-13	0.09%	1.021	0.008%	1.029	1.008	0.12%

Table 5. Summary of results for NACP-02 chamber simulations in graphite. All errors displayed are Type A and quote the standard uncertainty expressed as a percentage of the mean (k=1).

Energy (MeV)	Dose [Gy/source particle] full geometry ($D_{chamber}$)	Error	Dose [Gy/source particle] to graphite (D_g)	Error	$s_{g/air}$	Error	$D_g/D_{chamber}$	$p_{Q,g}$	$p_{Q,g}$ error
4	5.447E-14	0.05%	5.217E-14	0.07%	0.946	0.003%	0.958	1.013	0.08%
6	6.463E-14	0.05%	6.099E-14	0.07%	0.935	0.004%	0.944	1.009	0.08%
10	1.270E-13	0.06%	1.173E-13	0.07%	0.916	0.005%	0.923	1.008	0.09%
12	1.284E-13	0.07%	1.177E-13	0.07%	0.911	0.005%	0.917	1.006	0.10%
15	1.696E-13	0.07%	1.540E-13	0.07%	0.903	0.007%	0.908	1.005	0.10%
20	2.145E-13	0.06%	1.928E-13	0.08%	0.893	0.008%	0.899	1.007	0.10%

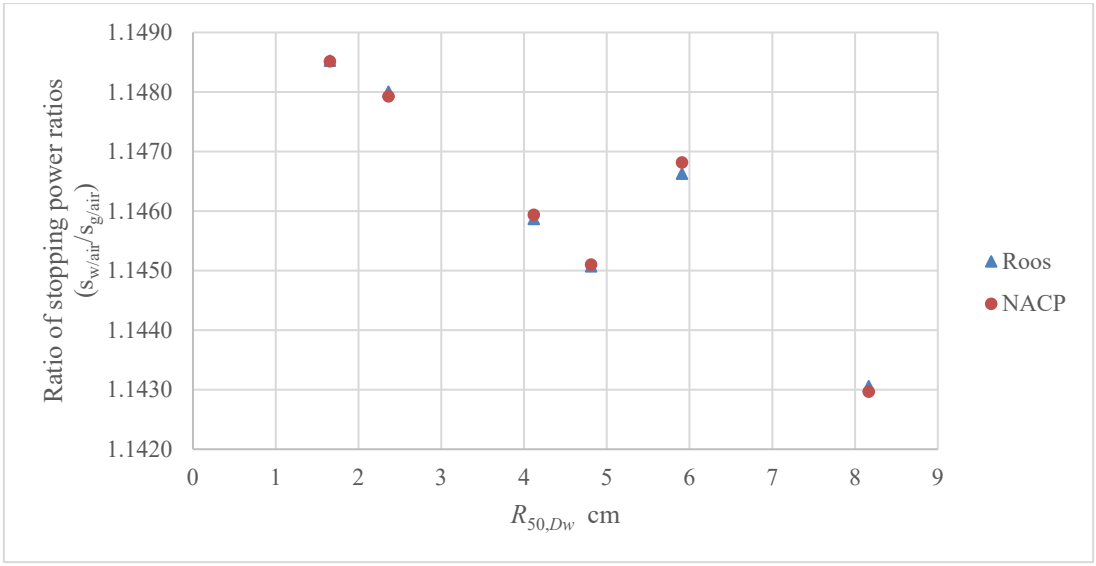

Figure 3 Graph showing the relationship between ratio of stopping power ratios ($s_{w/air}/s_{g/air}$) and $R_{50,Dw}$ for both Roos and NACP-02 chambers. Results for both chambers are virtually identical, as expected given the negligible differences in the simulations.

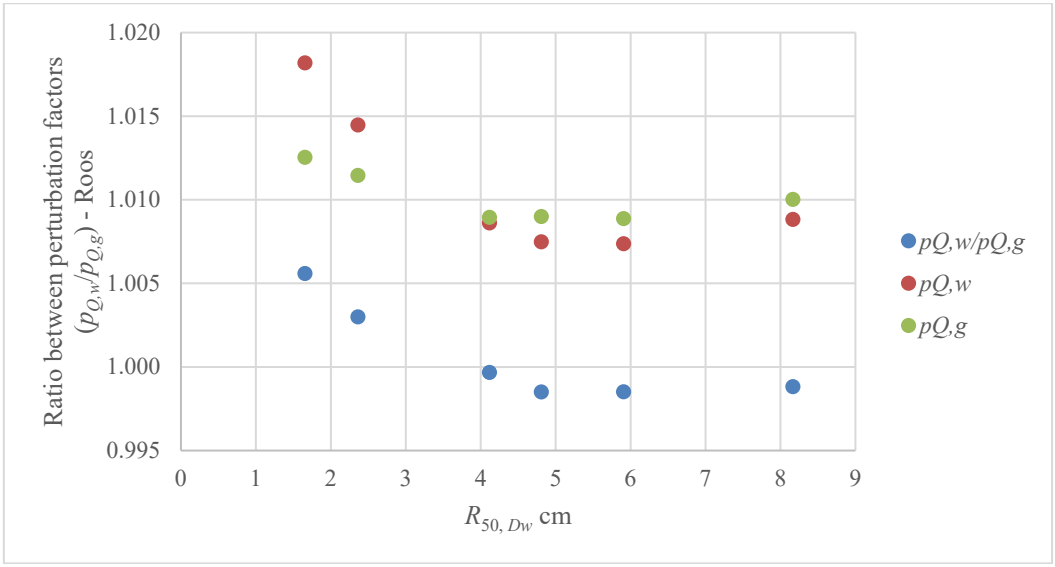

Figure 4. Graph showing the relationship between the ratio of $p_{Q,w}$ to $p_{Q,g}$ with respect to $R_{50,Dw}$ for the Roos chamber. Individual $p_{Q,w}$ and $p_{Q,g}$ values are also shown.

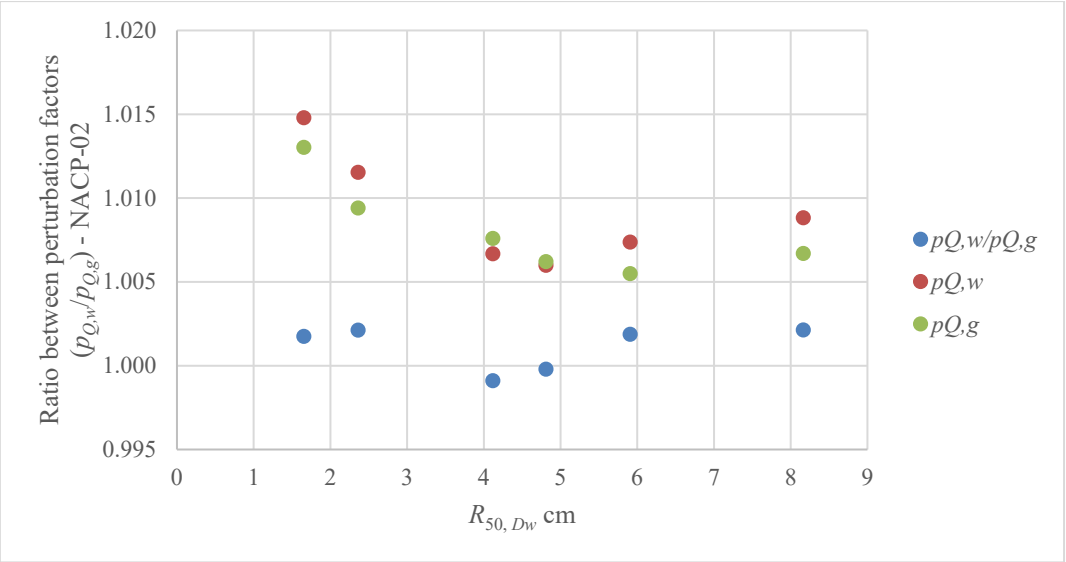

Figure 5. Graph showing the relationship between the ratio of $p_{Q,w}$ to $p_{Q,g}$ with respect to $R_{50,Dw}$ for the NACP-02 chamber. Individual $p_{Q,w}$ and $p_{Q,g}$ values are also shown.

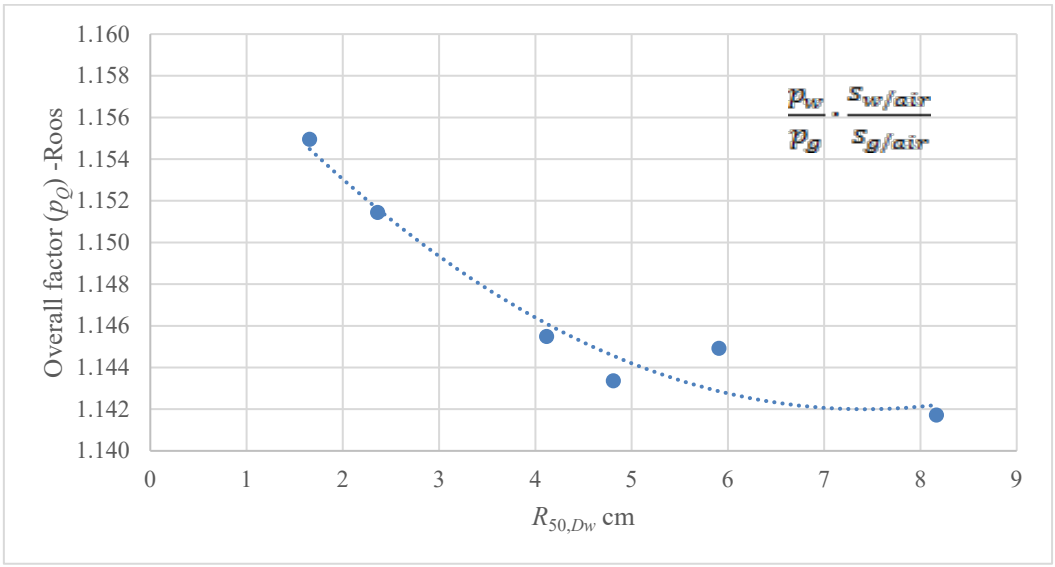

Figure 6. Graph showing the relationship between the overall factor p_Q (see Equation 6) with $R_{50,Dw}$ for the Roos chamber. This factor is applied to N_{Dg} (absorbed dose to graphite calibration factor) to convert to N_{Dw}. the absorbed dose to water calibration factor.

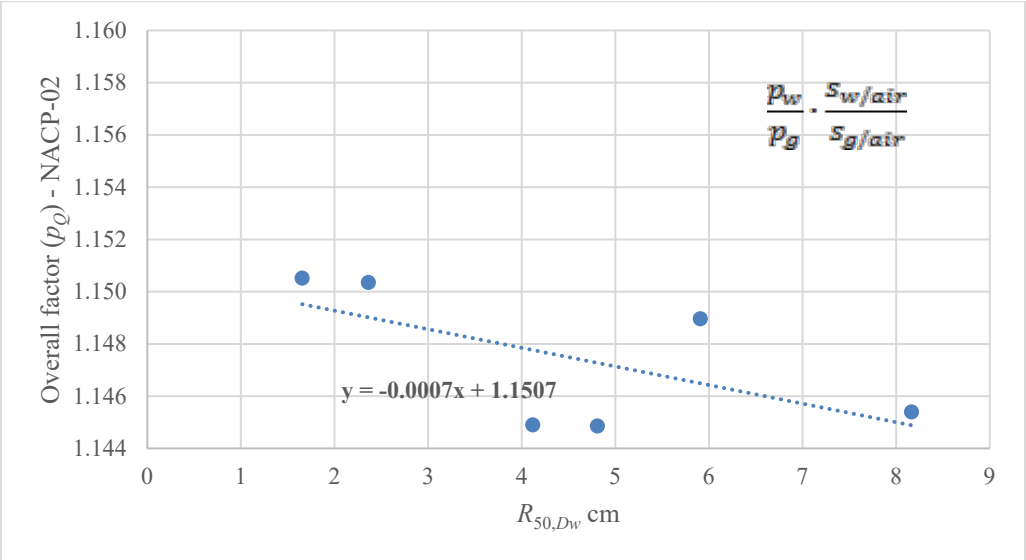

Figure 7. Graph showing the relationship between the overall perturbation factor p_Q (see Equation 6) with $R_{50,Dw}$ for the NACP-02 chamber. This factor is applied to N_{Dg} (absorbed dose to graphite calibration factor) to convert to N_{Dw}. the absorbed dose to water calibration factor.

Table 6. Final p_Q values calculated for the Roos chamber. These values are calculated using Equation 6 and the p_Q error is calculated in quadrature. All errors displayed are Type A and quote the standard uncertainty expressed as a percentage of the mean (k=1).

					Roos				
Energy (MeV)	**$R_{50,Dw}$ (cm)**	**$p_{Q,w}/p_{Q,g}$**	**Error $p_{Q,w}$**	**Error $p_{Q,g}$**	**$s_{w/air}$ / $s_{g/air}$**	**Error $s_{w/air}$**	**Error $s_{g/air}$**	**p_Q**	**Error p_Q**
4	1.656	1.006	0.11%	0.11%	1.149	0.002%	0.002%	1.155	0.15%
6	2.363	1.003	0.12%	0.11%	1.148	0.002%	0.002%	1.151	0.16%
10	4.118	1.000	0.12%	0.12%	1.146	0.003%	0.003%	1.145	0.17%
12	4.810	0.999	0.12%	0.12%	1.145	0.004%	0.003%	1.143	0.18%
15	5.909	0.999	0.11%	0.12%	1.147	0.007%	0.004%	1.145	0.17%
20	8.167	0.999	0.11%	0.14%	1.143	0.005%	0.006%	1.142	0.18%

Table 7. Final p_Q values calculated for the NACP-02 chamber. These values are calculated using Equation 6 and the p_Q error is calculated in quadrature. All errors displayed are Type A and quote the standard uncertainty expressed as a percentage of the mean (k=1).

					NACP-02				
Energy (MeV)	**$R_{50,Dw}$ (cm)**	**$p_{Q,w}/p_{Q,g}$**	**Error $p_{Q,w}$**	**Error $p_{Q,g}$**	**$s_{w/air}$ / $s_{g/air}$**	**Error $s_{w/air}$**	**Error $s_{g/air}$**	**p_Q**	**Error p_Q**
4	1.656	1.002	0.08%	0.08%	1.149	0.002%	0.003%	1.151	0.11%
6	2.363	1.002	0.10%	0.08%	1.148	0.002%	0.004%	1.150	0.13%
10	4.118	0.999	0.09%	0.09%	1.146	0.003%	0.005%	1.145	0.13%
12	4.810	1.000	0.10%	0.10%	1.145	0.003%	0.005%	1.145	0.14%
15	5.909	1.002	0.16%	0.10%	1.147	0.007%	0.007%	1.149	0.19%
20	8.167	1.001	0.15%	0.10%	1.143	0.008%	0.008%	1.145	0.18%

4 DISCUSSION

Prior to September 2019, it was assumed that the ratio between chamber perturbation factors (of specific chamber types NACP-02 and PTW Roos) in water $p_{Q,w}$ and in graphite $p_{Q,g}$ was unity. This ratio had never previously been calculated at NPL. Therefore, the conversion from chamber calibration factor in graphite (required for the calorimetry stage of the calibration process) to chamber calibration in water was previously attributed solely to differences in stopping power ratio. This report describes the work undertaken to calculate the perturbation factors for these chambers. In doing so, the updated data outlined in ICRU Report 90 relating to the physical properties of graphite and water were used. The overall p_Q factors at different energies were calculated for Roos and NACP-02 chambers using $p_{Q,w}$, $p_{Q,g}$ and stopping power ratios between the two media. The relationship between p_Q and $R_{50,Dw}$ was in agreement with previously collected measured data whereby SPR had been taken into account in the measurement process. Measured data was collected in the two measurement conditions (water and graphite) with efforts made to ensure the fluence at the measurement points were equivalent (e.g. z_{ref} corrected for water equivalent depth in the graphite set up and correction made for the inverse square law). The uncertainty in the experimentally derived values of p_Q was larger than desired, however their similarity with the factors calculated by Monte Carlo simulations was reassuring and served as an extra validation of these values. For some simulation geometries additional simulations were performed in order to keep the overall uncertainty in the factor calculated low. A small error in calculating the z_{ref} for the water simulations occurred and as such simulations were carried out with the correct z_{ref} for 15 MeV for both the NACP-02 and Roos chambers. Differences in the perturbation factors at the incorrect and correct z_{ref} were within the uncertainty of the calculation.

For both chamber types, applying the calculated factors in the conversion from dose to graphite to dose to water results in an increase in the chamber calibration coefficient at the lower energies transitioning to a decrease in the calibration coefficient at the higher energies, compared to previous values where the ratios of perturbation factors was assumed to be unity. This is slightly more pronounced for the Roos chamber at the lowest energies (+0.6% at 4 MeV) compared to the NACP-02 (+0.2% at 4 MeV), presumably due to the presence of graphite in the NACP-02 chamber. A separate NPL report (to be published) explores the comparison of NPL-calibrated chamber quality response compared to other published data.

5 CONCLUSION

The ratios of perturbation factors for reference parallel plate ionisation chambers of type NACP-02 and PTW Roos in graphite and water, previously assumed to be unity, were calculated for electron beam qualities over the nominal energy range 4-20 MeV incorporating the recommendations from ICRU Report 90. The resultant factors are significant enough to be introduced into the calibration process at NPL.

6 REFERENCES

1. Seltzer, S. M.;Fernandez-Varea, J. M.; Andreo, P.; Bergstrom, P. M.; Burns, D. T.; Krajcar Bronic, Ines; Ross, C. K.; Salvat F. Key data for ionizing-radiation dosimetry: measurement standards and applications, ICRU Report 90. J Int Comm Radiat Units Meas. 2016;14(1).
2. Berger MJ, Inokuti M, Anderson HH, Bichsel H, Dennis JA, Powers D, et al. Report 37. J Int Comm Radiat Units Meas. 1984 Dec 1;19(2):1–271.
3. McEwen MR, DuSautoy AR, Williams AJ. The calibration of therapy level electron beam ionization chambers in terms of absorbed dose to water. Phys Med Biol. 1998;43(9):2503–19.
4. Thwaites DI, DuSautoy AR, Jordan T, McEwen MR, Nisbet A, Nahum AE, et al. The IPEM code of practice for electron dosimetry for radiotherapy beams of initial energy from 4 to 25 MeV based on an absorbed dose to water calibration. Phys Med Biol. 2003;48(18):2929–70.
5. Bailey M, Shipley DR, Manning JW. Roos and NACP-02 ion chamber perturbations and

water-air stopping-power ratios for clinical electron beams for energies from 4 to 22 MeV. Phys Med Biol. 2015;60(3):1087–105.

6. Burns DT, Ding GX, Rogers DWO. R 50 as a beam quality specifier for selecting stopping-power ratios and reference depths for electron dosimetry. Med Phys [Internet]. 1996 Mar;23(3):383–8. Available from: http://doi.wiley.com/10.1118/1.597893
7. Bass, G. A.; Barry, M.A.; Duane, S.; Homer, M. J.; Kelly, M.; Manning, J. W.; Maughan, D. J.; Nutbrown, R. F.; Sander, T.; Shipley, D. R.; Snaith JAD. NPL Report IR 55: Changes to the UK National Primary Standards of air kerma and absorbed dose incorporating ICRU Report 90 recommendations. 2019.
8. Kawrakow I, Rogers DWO, Mainegra-Hing E, Tessier F, Townson RW, Walters BRB. EGSnrc toolkit for Monte Carlo simulation of ionizing radiation transport. Technical Report. 2000 v2018.

7 APPENDICES

7.1 APPENDIX A

Additional work was carried out to determine the suitability of phantom size for the water simulations. Simulations described in Sections 2.3 and 2.4 were carried out for both 15 and 20 MeV using a phantom radius of both 8 cm and 15 cm in water. No additional calculations were carried out for the graphite simulations. Data collected are displayed in Tables 8, 9, 10 and 11. The results showed that there was a very small increase in D_w and the corresponding $p_{Q,w}$ data using a radius of 15 cm as opposed to 8 cm for the 20 MeV simulation in water. For the 15 MeV simulation in water there was no significant change in the results using radius of 15 cm as opposed to 8 cm. Therefore, for all energies of less than 15 MeV, the original data obtained using the smaller phantom radius of 8 cm were used.

Table A1. Summary of results for Roos chamber simulations in water for 15 and 20 MeV for different phantom sizes. All errors displayed are Type A and quote the standard uncertainty expressed as a percentage of the mean (k=1).

						Roos				
Energy (MeV)	**Phantom radius**	**Dose [Gy/source particle] full geometry ($D_{chamber}$)**	**Error**	**Dose [Gy/source particle] to water (D_w)**	**Error**	**$s_{w/air}$**	**Error**	**$D_w/D_{chamber}$**	**$p_{Q,w}$**	**$p_{Q,w}$ error**
15	8 cm	1.174E-13	0.12%	1.224E-13	0.08%	1.036	0.004%	1.043	1.007	0.14%
	15 cm	1.175E-13	0.08%	1.226E-13	0.08%	1.036	0.007%	1.043	1.007	0.11%
20	8 cm	2.091E-13	0.12%	2.149E-13	0.08%	1.021	0.005%	1.028	1.007	0.14%
	15 cm	2.091E-13	0.08%	2.153E-13	0.08%	1.021	0.005%	1.030	1.009	0.11%

Table A2. Summary of results for NACP-02 chamber simulations in water for 15 and 20 MeV for different phantom sizes. All errors displayed are Type A and quote the standard uncertainty expressed as a percentage of the mean (k=1).

						NACP-02				
Energy (MeV)	**Phantom radius**	**Dose [Gy/source particle] full geometry ($D_{chamber}$)**	**Error**	**Dose [Gy/source particle] to water (D_w)**	**Error**	**$s_{w/air}$**	**Error**	**$D_w/D_{chamber}$**	**$p_{Q,w}$**	**$p_{Q,w}$ error**
15	8 cm	1.176E-13	0.08%	1.226E-13	0.08%	1.036	0.005%	1.042	1.006	0.11%
	15 cm	1.175E-13	0.11%	1.226E-13	0.12%	1.036	0.007%	1.044	1.008	0.16%
20	8 cm	2.096E-13	0.06%	2.150E-13	0.08%	1.021	0.005%	1.025	1.005	0.10%
	15 cm	2.095E-13	0.09%	2.156E-13	0.09%	1.021	0.008%	1.029	1.008	0.12%

Table A3. Final p_Q value calculated for the Roos chamber for 15 and 20 MeV for different phantom sizes. These values are calculated using Equation 6 and the p_Q error is calculated in quadrature. All errors displayed are Type A and quote the standard uncertainty expressed as a percentage of the mean (k=1).

Energy (MeV)	$R_{50,Dw}$ (cm)	Phantom radius	Roos							
			$p_{Q,w}/p_{Q,g}$	Error $p_{Q,w}$	Error $p_{Q,g}$	$s_{w/air}$ / $s_{g/air}$	Error $s_{w/air}$	Error $s_{g/air}$	p_Q	Error p_Q
15	5.909	8 cm	0.998	0.14%	0.12%	1.147	0.004%	0.004%	1.144	0.19%
		15 cm	0.999	0.11%	0.12%	1.147	0.007%	0.004%	1.145	0.17%
20	8.167	8 cm	0.997	0.14%	0.14%	1.143	0.005%	0.006%	1.140	0.20%
		15 cm	0.999	0.11%	0.14%	1.143	0.005%	0.006%	1.142	0.18%

Table 8. Final p_Q value calculated for the NACP-02 chamber for 15 and 20 MeV for different phantom sizes. These values are calculated using Equation 6 and the p_Q error is calculated in quadrature. All errors displayed are Type A and quote the standard uncertainty expressed as a percentage of the mean (k=1).

Energy (MeV)	$R_{50,Dw}$ (cm)	Phantom radius	NACP-02							
			$p_{Q,w}/p_{Q,g}$	Error $p_{Q,w}$	Error $p_{Q,g}$	$s_{w/air}$ / $s_{g/air}$	Error $s_{w/air}$	Error $s_{g/air}$	p_Q	Error p_Q
15	5.909	8 cm	1.001	0.11%	0.10%	1.147	0.005%	0.007%	1.148	0.15%
		15 cm	1.002	0.16%	0.10%	1.147	0.007%	0.007%	1.149	0.19%
20	8.167	8 cm	0.998	0.10%	0.10%	1.143	0.005%	0.008%	1.141	0.14%
		15 cm	1.001	0.15%	0.10%	1.143	0.008%	0.008%	1.145	0.18%